DOI: 10.1002/cbic.201900358

Enzymatic Route toward 6-Methylated Baeocystin and Psilocybin

Janis Fricke,[a] Alexander Sherwood,[b] Robert Kargbo,[b] Andrew Orry,[c] Felix Blei,[a] Andreas Naschberger,[d] Bernhard Rupp,[d, e] and Dirk Hoffmeister*[a]

Psilocybin and its direct precursor baeocystin are indole alkaloids of psychotropic *Psilocybe* mushrooms. The pharmaceutical interest in psilocybin as a treatment option against depression and anxiety is currently being investigated in advanced clinical trials. Here, we report a biocatalytic route to synthesize 6-methylated psilocybin and baeocystin from 4-hydroxy-6-methyl-L-tryptophan, which was decarboxylated and phosphorylated by the *Psilocybe cubensis* biosynthesis enzymes PsiD and PsiK. N-Methylation was catalyzed by PsiM. We further present an in silico structural model of PsiM that revealed a well-conserved SAM-binding core along with peripheral non-conserved elements that likely govern substrate preferences.

The indole nucleus is a common motif with bioactive natural products that is, in numerous instances, modified during biosynthesis. Modifications include, for example, 7-chlorination in the case of rebeccamycin, prenyl transfer to various positions to make asterriquinones, or hydroxylation at C-5 and C-6 of serotonin and amanitins, respectively. Reserpine, ibogaine, and harmaline are methoxy-substituted at these carbons. Dissimilar from the above positions and substituents, psilocybin (**1**, Scheme 1) features a unique 4-phosphoryloxy group.

Compound **1** is the principal metabolite of *Psilocybe* carpophores ("magic mushrooms"), whereas baeocystin (**2**) and norbaeocystin (**3**), the immediate metabolic precursors, are present in minor quantities.[1] The dephosphorylated analogue of **1**, psilocin (**4**), represents the pharmacologically active, that is, psychotropic compound as it is a partial agonist at the human $5HT_{2A}$ receptor.[2] The pharmaceutical value of **1** in the treatment of end-of-life anxiety and therapy refractory depression has been documented in various advanced clinical trials.[3] Syntheses of **1** congeners date back to the late 1950s. Following the discovery of **1** by Albert Hofmann and co-workers, various series of derivatives were synthesized, which also contained the 6-phosphoryloxy and 6-hydroxy isomers of **1** and **4**, along with a 6-methylated, side-chain-alkylated tryptamine.[4] Subsequent efforts were made to install bromine or a formyl group at C-5- or C-7, vary the substituents at the ω-N-atom of **4**, or add various substituents to the aromatic ring of *N*,*N*-dimethyltryptamine (**5**), to produce its 6- and 7-methyl analogues, among others.[5] Despite these results and despite the synthesis of 2-methyl derivatives of **5** and *N*,*N*-diethyltryptamine,[6] none of the previous efforts, using synthetic chemistry, had focused on introducing a methyl substituent to the indole of **1** or **2**.

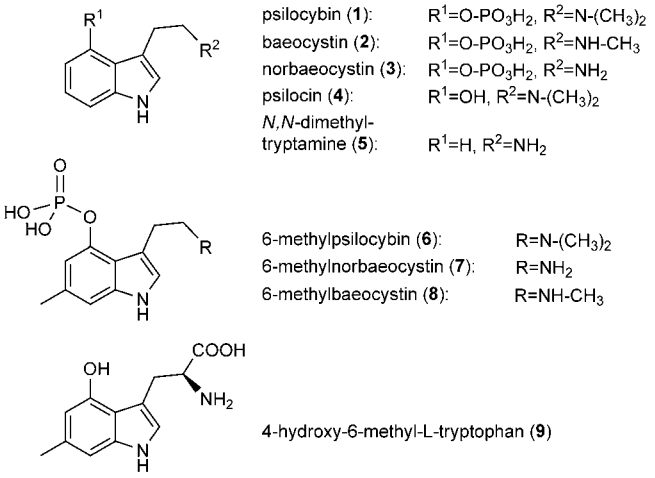

Scheme 1. Chemical structures of psilocybin and other naturally occurring or synthetic L-tryptophan derivatives relevant to this study.

We report the in vitro synthesis of 6-methylpsilocybin (**6**, Scheme 1) and, as main products, its immediate precursors 6-methylnorbaeocystin (**7**) and 6-methylbaeocystin (**8**). We address the previous lack of ring-methylated **1** analogues and simultaneously provide a model of the PsiM structure for insight into the origin of its methylating activity on **3** and **7**. We identified a loop structure as critical for methyl acceptor substrate selectivity. Concurrent site-directed *psiM* mutagenesis experimentally validated the structural model.

Four enzymes, the decarboxylase PsiD, the P_{450} monooxygenase PsiH, the kinase PsiK, and the iteratively acting *N*-methyltransferase PsiM, confer the capacity to biosynthesize **1**.[7] Based on this finding, a biocatalytic route was reported that

[a] *J. Fricke, F. Blei, Prof. Dr. D. Hoffmeister*
Department Pharmaceutical Microbiology at the Hans Knöll Institute
Friedrich-Schiller-Universität
Beutenbergstrasse 11a, 07745 Jena (Germany)
E-mail: dirk.hoffmeister@leibniz-hki.de

[b] *Dr. A. Sherwood, Dr. R. Kargbo*
The Usona Institute
2800 Woods Hollow Road, Madison, WI 53711 (USA)

[c] *Dr. A. Orry*
Molsoft L.L.C.
11199 Sorrento Valley Road, San Diego, CA 92121 (USA)

[d] *Dr. A. Naschberger, Dr. B. Rupp*
Department of Genetic Epidemiology, Medizinische Universität Innsbruck
Schöpfstrasse 41, 6020 Innsbruck (Austria)

[e] *Dr. B. Rupp*
Hofkristallamt
991 Audrey Place, Vista, CA 92084 (USA)

Supporting information and the ORCID identification numbers for the authors of this article can be found under https://doi.org/10.1002/cbic.201900358.

makes use of tryptophan synthase *P. cubensis* TrpB, alongside PsiD, PsiK, and PsiM, to produce **1** in vitro from 4-hydroxyindole and L-serine.[8] The intrinsic substrate flexibility of TrpB, PsiD, and—to a lesser extent—PsiK, allowed successful conversion of 5- and 7-hydroxyindole into serotonin or isonorbaeocystin (=7-phosphoryloxynorbaeocystin). However, the strictly specific methyltransferase PsiM prevented further turnover, and 6-hydroxyindole processing failed altogether at the initial TrpB-catalyzed step. We re-investigated the above enzymatic route and tested if recombinantly produced *P. cubensis* TrpB converted 4-hydroxy-6-methylindole (**10**), together with L-serine as second substrate, to 4-hydroxy-6-methyl-L-tryptophan (**9**, Scheme 1). However, UHPLC/MS analysis did not indicate product formation (Figure 1 A), whereas a positive control with indole and L-serine yielded L-tryptophan, as expected. The assay was repeated with TRP5, the tryptophan synthase of baker's yeast (*Saccharomyces cerevisiae*).[9] Its 2124 bp cDNA was cloned to heterologously produce the enzyme (monomeric mass of the N-terminally hexahistidine-tagged fusion protein: 79.1 kDa, Figure S1 in the Supporting Information). In the TRP5-containing assays, product formation was observed, albeit at low yields (Figure 1 B).

Previously, *Salmonella enterica* tryptophan synthase had been shown to accept 6-methylindole as substrate.[10] As disubstituted indoles had not been tested then, we included this enzyme in our in vitro study. The positive control was run with unsubstituted indole. A product peak at $t_R = 3.8$ min, with a mass of *m/z* 235.1 $[M+H]^+$ and a tryptophan-like UV/Vis spectrum, indicated successful conversion of **10** into **9** (Figure 1 C).

To scale up the production for subsequent reactions, we continued with the *S. enterica* enzyme to produce **9**. It was used for a one-pot reaction with recombinantly produced and N-terminally hexahistidine-tagged PsiD, PsiK, PsiM, and the appropriate co-substrates (Scheme 2). Substrate **9** was added at

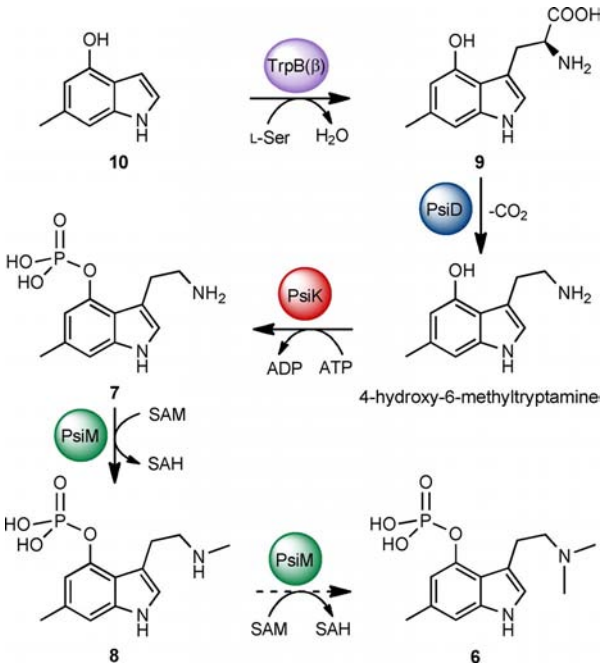

Scheme 2. Enzymatic synthesis of 4-hydroxy-6-methyl-L-tryptophan (**9**) by *S. enterica* tryptophan synthase and subsequent conversion by *P. cubensis* decarboxylase PsiD, kinase PsiK, and methyltransferase PsiM into 6-methylnorbaeocystin (**7**), 6-methylbaeocystin (**8**), and 6-methylpsilocybin (**6**). The dashed arrow indicates low turnover to **6**.

1 mM to the reaction. After 4 h of incubation, UHPLC/MS analysis unequivocally detected two major new compounds that showed the typical tryptophan fingerprint UV/Vis spectrum, and a third compound in trace quantity. The first signal (t_R = 1.4 min, Figure 2) corresponded to a mass of *m/z* 271.0842 $[M+H]^+$, the second one (t_R = 2.1 min) to *m/z* 285.0998 $[M+H]^+$. These two masses are identical to those of **2** and **1**.

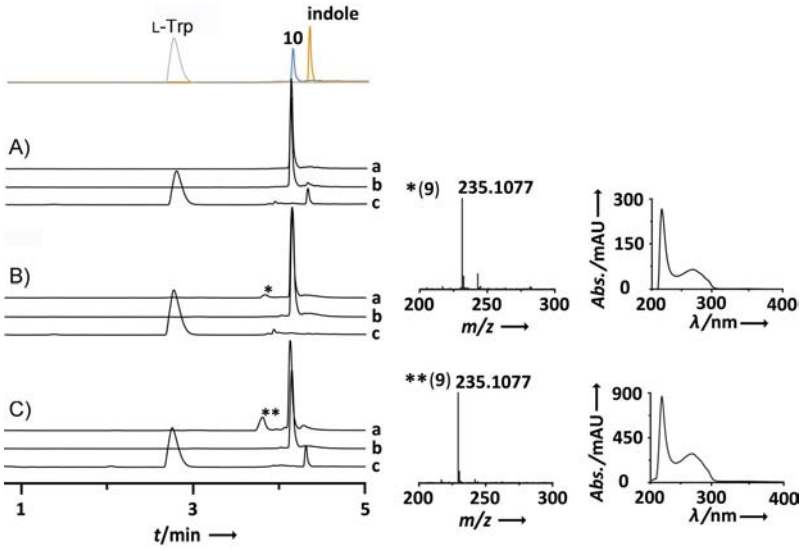

Figure 1. Formation of 4-hydroxy-6-methyl-L-tryptophan (**9**) by tryptophan synthases. Chromatograms were recorded at $\lambda = 280$ nm, HRMS(ESI) spectra were recorded in positive mode. Top: overlaid individual chromatograms of authentic reference compounds. Reactions with A) *P. cubensis* TrpB, B) *S. cerevisiae* TRP5, and C) *S. enterica* tryptophan synthase. Traces a: enzymatic reaction, b: negative controls with heat-treated enzyme, c: positive control yielding L-tryptophan. Right: UV/Vis spectra of the peaks marked with asterisks.

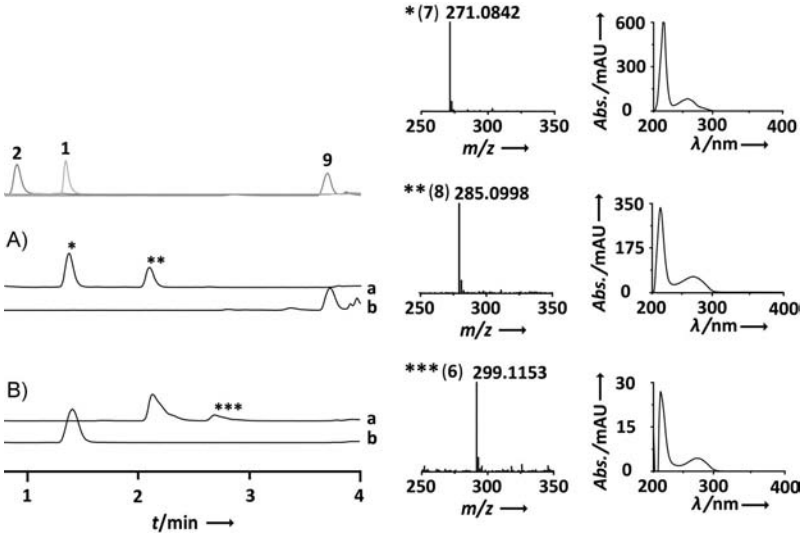

Figure 2. Analysis of enzymatic assays to produce 6-methylated psilocybin and congeners. Chromatograms were recorded at $\lambda = 280$ nm, HRMS(ESI) spectra were recorded in positive mode. Top: overlaid individual chromatograms of reference compounds. Reactions with A) PsiD, PsiK, and PsiM; B) 6-methylnorbaeocystin (**7**) and PsiM, SAH nucleosidase, and adenine deaminase. Traces a: enzymatic reaction, b: negative controls with heat-treated enzyme. Minor additional signals around 4.0 min are follow-up products of instable **9**. Retention times and other details are shown in Table S1. Right: UV/Vis spectra of the peaks marked with asterisks.

However, due to dissimilar retention times ($t_R = 0.9$ and 1.4 min) of authentic **2** and **1**, we could discount the possibility that these known tryptamines had been formed. The above masses were also compatible with **8** and its precursor **7**. A negative control with heat-treated enzymes did not show turnover (Figure 2).

For further verification, MS/MS analysis was performed (Figure S2). Fingerprint fragments typical for **1** and related tryptamines were detected: besides the phosphate group, the fragment losses for the side-chain amino group—H_3N in **7**, CH_3NH_2 in **8**, and $(CH_3)_2NH$ in **6**—were found. These losses verified the primary amine of **7**, and the degree of N-methylation in **8** and **6**. Furthermore, the detected fragment ions 162.0915 for $(C_{10}H_{12}NO)^+$ and 174.0915 for $(C_{11}H_{12}NO)^+$ were consistent with retention of the methyl and hydroxy substitution on the indole core provided by substrate **10**.

Additionally, an scaled-up enzymatic reaction with PsiD, PsiK and, separately, with PsiM was carried out that yielded approximately 1 mg of compound after partial chromatographic purification. Subsequent 1D and 2D ^{1}H NMR analysis provided evidence supporting the successful biocatalytic synthesis of **8**. The ^{1}H NMR and COSY spectra (Figures S3 and S4) revealed three aromatic signals as well as a singlet at 10.71 ppm, indicative of the H-1 indole N-H, each with an integration value corresponding to one proton. The singlet at 6.99 ppm corresponded to H-2, and distinct singlet signals at 6.83 and 6.64 ppm corresponded to H-5 and H-7, respectively. Finally, a singlet that integrated to 3 H at 2.32 ppm was consistent with the methyl group attached to position 6 of the indole core. COSY revealed coupling between indole protons H-1 and H-2. Additionally, a weak long-range coupling was observed between the aromatic methyl singlet at 2.32 ppm and the *ortho*-aromatic proton H-5 at 6.83 ppm (Scheme 3).

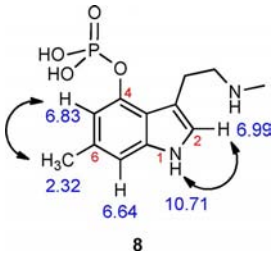

8

Scheme 3. Selected ^{1}H NMR shifts (blue) and COSY correlations (black arrows) supporting the structural assignment of **8**.

The above data, taken collectively with high-resolution mass spectra, provided strong support for the structural assignment of **8** made by biocatalytic synthesis. Still, our triple-enzyme process had primarily yielded a monomethylated, that is, secondary amine (Figure 2 A), while the N,N-dimethylated product **6** was formed only in traces.

To exclude the possibility that *S*-adenosyl-L-homocysteine (SAH), the second product of the PsiM reaction, might have accumulated and inhibited the second methyltransfer, the PsiM reaction was repeated as a single-enzyme assay with **8** as substrate and in the presence of SAH nucleosidase and adenine deaminase. This procedure irreversibly eliminates SAH from the equilibrium. Still, the N,N-dimethylated product **6** was detected only in minor amounts under these conditions and identified by LC/MS (Figure 2 B). This observation contrasts with other methyltransferases that act on α-amino groups during natural product assembly. The well-understood gateway enzyme of the mycobacterial ergothioneine pathway, EgtD,[11] catalyzes L-histidine trimethylation.

In the crystal structure of EgtD, residue Asn166 was recognized as being essential to making the *N*,*N*-α-dimethyl-L-histi-

dine intermediate a 100-fold stronger ligand than L-histidine itself, which promotes trimethylation. A similar enzyme, Ybs of *Aspergillus nidulans*, preferentially trimethylates L-tyrosine, but also L-histidine, L-DOPA, and L-phenylalanine.[11a] The phylogenetically related *Psilocybe serbica* methyltransferase TrpM, which is not part of **1** biosynthesis, dimethylates the amino groups of L-tryptophan, L-tyrosine, and L-phenylalanine, but transfers a third methyl group only very poorly.[12] Despite their being substrate flexible, kinetics and affinity determine the number of methyl groups transferred by the above enzymes, whereas the number of catalytic cycles was independent of the acceptor compound. Here, turnover with *P. cubensis* PsiM, an established *N*,*N*-dimethyltransferase acting on **3**, strongly decreases after one methyltransfer when **8** is offered as substrate.

To address this phenomenon more profoundly, the PsiM structure was modeled. PsiM is a class I *S*-adenosyl-L-methionine (SAM)-dependent natural product *N*-methyltransferase and is active as a monomer, as shown by size-exclusion chromatography (Figure S5). Methyltransferases share a common Rossmann-like fold containing the SAM binding site with a highly conserved xGxG motif in a turn and a carboxylate residue anchoring the nucleoside ribose of SAM,[13] but often share as little as 10% sequence identity.[14] Interestingly, PsiM has no basic sequence similarity to the *N*-methyltransferases involved in tryptamine methylation in neurotransmitter biosynthesis, such as human phenylethanolamine *N*-methyltransferase (hPNMT). In contrast, PsiM shows sequence identity of ≈40% with human small nuclear RNA MTs (METTL16) and human MT 10 domain containing protein (annotated as METT10D and including residues 40–291 of METTL16). Basic SwissModel threading models[15] expectedly show reasonable quality in the Rossman fold core (residues 37–188 and 222–289), but uncertainty remains in the poorly aligned loop and N-terminal region.

We selected the SAH-containing high-resolution X-ray structure PDB ID: 2H00[16] with 43% sequence identity as a template for homology modeling with ICM Pro and used the SAH pose of 2H00 as initial starting template for SAM docking (Figures 3 and S6).

The model shows that access to the conserved Rossmann-like SAM-harboring fold is likely determined by the central loop domain, which, in absence of a template structure, cannot be reliably modeled. The role of the N-terminal extension distal to the SAM-binding site is also unknown for PsiM, and the model must remain tentative. In the well-conserved core structure, the leaving methyl group of SAM is fittingly extending from the binding pocket into the lumen of the pocket environment (Figures 3 and S7), and the extraordinary specificity of PsiM must necessarily originate in the structural details of the remaining pocket-forming and substrate-presenting groups as well as protein side chains of the loop domain. As PsiM's substrate specificity is largely determined by the additional nonconserved structure parts that cannot be reliably modeled, any in silico substrate docking based on a homology model remains speculative, and a structural basis for the different activities of PsiM for 6-substituted tryptamines versus non-

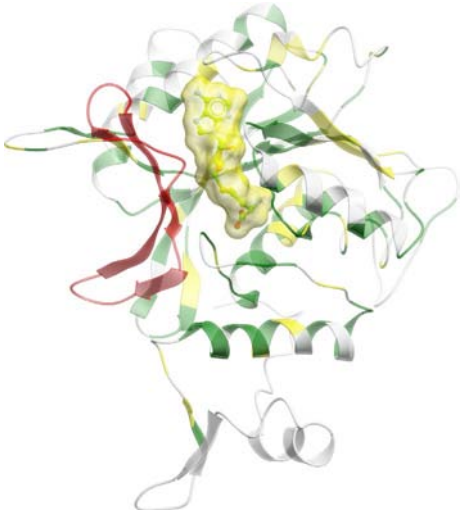

Figure 3. Homology modeling of *P. cubensis* PsiM (ribbons) with docked SAM (ball and stick model in yellow macrosphere) showing the conservation of the Rossmann-fold like core. The model ribbon is colored according to sequence conservation with the template structure PDB 2H00. Green: conserved, yellow: semi-conserved, white: non-conserved, red: no template structure available. The Rossmann-like fold harboring the SAM is well conserved, whereas the N-terminal region (gray helix at the bottom) and the modeled loop from approximately residues 189 to 221 with no template structure (red) must be considered tentative.

or 4-substited tryptamines remains elusive. The PsiM crystal structure, preferably in complex with products, substrates, or analogues, will be necessary to accurately determine the actual origin of the functional specificity, including why 6-substituted trypamines are not well processed by PsiM beyond the first methylation step.

For a first experimental validation of our structure model, we mutated the *psiM* gene to individually replace R75, D161, N183, Y187, S196, and H210 by an alanine residue. According to our model (Figure S7), four positions are located in the well-supported part of the model, with R75, N183, and Y187 being directly involved in SAM binding, although the contribution of solvent-exposed D161 to SAM binding was unclear. The engineered enzymes were heterologously produced as hexahistidine fusion proteins (Figure S8), purified, and tested for activity in vitro. Consistent with the model, the D161A variant was as active as the wild-type enzyme in in vitro assays. Variants R75A, N183A, and Y187A were catalytically inactive, as expected, most likely due to impaired SAM binding. Another two residues (S196 and H210) might also be involved in SAM binding, but are located in the loop region that, in the absence of a template, cannot be reliably modeled but that most likely confers methyl-acceptor specificity on PsiM. Variant S196A was inactive as well, perhaps as consequence of a destabilizing effect on the loop. Remarkably, H210A showed a near-normal first methylation of the standard substrate **3** into **2**, yet failed to perform the second methylation of **2** into **1** (Figure S9). Likewise, **6** was not detected in the in vitro reactions, whereas **8** was formed, albeit in low amounts. The reason for this shift in activity remains elusive but seems to underscore the relevance of the loop region for substrate recognition.

In conclusion, we have shown the enzymatic in vitro synthesis of the 6-methylated psilocybin congeners **6**–**8**. Indole methylation at carbon atom 6 does not cause consistent pharmacological effects. A study on 5-HT_{2B} receptor antagonists involving tetrahydro-β-carbolines showed that 6-methylation moderately impacted receptor binding and increased affinity eightfold.[17] In a series of synthetic chlorophenylethanol-substituted indolylalkylamine β_3-adrenergic receptor agonists, indole methylation at C-6 did not alter affinity and led to comparable agonistic activity.[18] Conversely, unlike its parental compound **5**, the 6-methylated analogue did not interact competitively with serotonin receptors.[5c]

Compound **1** is a candidate drug to treat depression and is being investigated in clinical trials, and gram-scale production of **1** by chemical synthesis has been described, as well as production in submerged culture.[19] Our future efforts are directed to a scale-up to provide sufficient **6** and **7** by biocatalytic means in vitro for comparative in vivo assays, in particular to discover agonistic or antagonistic effects on 5-HT receptors and, ultimately, for more profound insight into the pharmacology of serotonergic psychedelics.

Experimental Section

General procedures: Plasmid isolation, DNA restriction, and ligation followed the instructions of the manufacturers of kits and enzymes (NEB, Promega, Thermo, Zymo). Chemicals, media ingredients, and solvents were purchased from Becton–Dickinson, Key Organics, Roth, Sigma–Aldrich, THC Pharm, VWR, and Deutero. Oligonucleotides were synthesized by Microsynth.

Cloning of *S. cerevisiae* TRP5: *S. cerevisiae* BY4741 (Euroscarf) was grown in shaken liquid YPD medium (per liter: 10 g yeast extract, 20 g peptone, 20 g D-glucose). After harvest, total RNA was isolated by using the SV Total RNA isolation kit (Promega). Synthesis of the first cDNA strand was primed with an oligo-d(T)-primer and RevertAid reverse transcriptase. A subsequent PCR with oligonucleotide primers (0.2 μM each) oJF127 (5′-TATAT AGCTA GCCAT GTCAG AACAA CTCAG-3′, NheI site underlined) and oJF128 (5′-TATAT ACTCG AGTTA GGCAG ATGGG TC-3′, XhoI site underlined) completed synthesis of the second strand. The PCR was set up with 0.2 mM each dNTP, 2 mM $MgSO_4$, in HF buffer that was supplied with the enzyme (Phusion DNA polymerase, 1 U). The PCR product was electrophoretically purified, subsequently extracted from an agarose gel, and ligated between the NheI and XhoI sites of pET28a, to create expression plasmid pJF56.

Mutation of PsiM: Site-directed mutagenesis of the *psiM* gene was accomplished by PCR amplifying the gene from pET28-based expression plasmid pFB13[7a] as template. Each gene variant was amplified in two fragments that overlapped in the portion to be mutated. The 5′-end of fragment 1 and the 3′-end of fragment 2 overlapped with the polylinker of plasmid pET28a, linearized by BamHI and HindIII restriction enzymes. Plasmids were assembled with the NEBuilder HiFi DNA Assembly Kit to yield constructs pJF71-76 for variants R75A, D161A, N183A, Y187A, S196A, and H210A, respectively. Primers for PCR amplifications of fragments 1 included forward oligonucleotide oJF161 and reverse oligonucleotides oJF163, oJF165, oJF167, oJF169, oJF171, or oJF173. Fragments 2 were amplified with reverse primer oJF162 and forward primers oJF164, oJF166, oJF168, oJF170, oJF172, or oJF174. Primer sequences are shown in Table S2.

Heterologous protein production and purification: All enzymes were produced in *Escherichia coli* KRX (Promega). *Psilocybe* enzymes TrpB, PsiD, PsiM, and PsiK were produced as described.[7a,8] For heterologous production of *S. cerevisiae* TRP5, *E. coli* KRX transformed with pJF56 was used. Production of *E. coli S*-adenosylhomocysteine nucleosidase and adenine deaminase followed a described procedure.[11b,12] The above enzymes were purified by immobilized metal-affinity chromatography on a His Trap FF Crude column (1 mL bed volume), fitted to an Äkta Pure 25 FPLC instrument (GE Healthcare). The system was equilibrated in loading buffer (50 mM sodium dihydrogen phosphate, 300 mM NaCl, 20 mM imidazole, pH 8). The column was washed by a step gradient of 30, 40, and 50 mM imidazole, using the same buffer. Elution was at 500 mM imidazole. The flow rate was 1 mL min^{-1}. For later use in assays, the eluted enzymes were rebuffered on PD-10 columns (GE Healthcare), equilibrated with Tris·HCl buffer (50 mM, pH 8.0). *S. enterica* tryptophan synthase was also produced in *E. coli* KRX, transformed with plasmid pSTB7, but enzymatic reactions were run with the cell lysate.[10] The biomass from a 500 mL culture was harvested by centrifugation (1200 *g*, 4 °C, 20 min), and the cell paste was resuspended in sonication buffer (7 mL, 500 mM Tris·HCl, 5 mM EDTA, 10 mM β-mercaptoethanol, 1 mM PMSF, 100 μM PLP, pH 7.8), sonicated, and centrifuged again (14000 *g*, 4 °C, 20 min) to remove cell debris. For subsequent reactions (below), 100 μL of the supernatant containing cell lysate was used. For size-exclusion chromatography with intact and heat-treated PsiM, samples were loaded onto a Superdex 200 column and eluted with 10 mM phosphate buffer with 140 mM NaCl.

Enzyme assays: All reactions were carried out in triplicate. In vitro tryptophan synthase assays with *P. cubensis* TrpB were carried out as described.[8] Reactions with TRP5 (1 μM) were run in a volume of 500 μL and buffered in Tris·HCl (50 mM, pH 8.0). L-Serine and **10** (or indole in the positive control) were added at 1 mM each, PLP at 100 μM final concentration. The assay mixtures were incubated over night at room temperature (37 °C for the *S. enterica* enzyme), lyophilized, resuspended in methanol (200 μL), filtered, and chromatographically analyzed (below). The assays with the *S. enterica* enzyme were run identically, but with cell lysate. To prepare **9** in a scaled-up reaction, the procedure by Goss and Newill was applied.[10]

The triple-enzyme assay (PsiD/PsiK/PsiM) was buffered in phosphate buffer (50 mM, pH 7.5) and incubated at ambient temperature for 4 h. It contained ATP, $MgCl_2$, and SAM (2 mM each), **9** (1 mM), and enzyme (1 μM each). The total volume was 300 μL. A separate assay was set up with SAM (2 mM), **7** (1 mM), PsiM (1 μM), and *E. coli* adenine deaminase und SAH nucleosidase (1 μM each). To prepare **8** for NMR-based structure elucidation, a combined PsiD/PsiK assay (1 μM each enzyme, phosphate buffer, pH 7.5, 4 h, room temperature) was carried out that contained ATP and $MgCl_2$ (2 mM each), and **9** (1 mM) in a volume of 30 mL. Product **7** was purified chromatographically (below). To complete production of **8**, a subsequent separate reaction was run (1 mM) PsiM, Tris·HCl buffer, pH 8.0, for 4 h, room temperature) that contained SAM (2 mM) and **7** (1 mM) in a volume of 30 mL. Reactions were stopped by freezing, and the mixtures subsequently lyophilized, solved in 200 μL MeOH (50 mL in case of preparative assays to produce **8**), centrifuged (14000 *g*, 4 °C, 10 min), and filtered to prepare them for chromatography (below).

Chemical analysis of enzyme assays: All UHPLC/ESIMS analyses of in vitro assays were performed on an Agilent Infinity 1290 chromatograph with a Phenomenex Luna Omega C_{18} column (100× 2.1 mm, 1.6 μm particle size, flow: 0.5 mL min^{-1}), coupled to an Agi-

lent 6130 Single Quadrupole mass detector. Diode array detection was between $\lambda = 200–400$ nm. Chromatograms were extracted at $\lambda = 280$ nm. Solvent A was 0.1% (*v/v*) formic acid in H_2O, solvent B was acetonitrile (ACN). The linear gradient was 1→10% B over 3 min, then →100% B over 1 min. LC/HRESIMS, and MS/MS analyses with purified substances were performed on a Thermo Accela chromatograph coupled to an Exactive Orbitrap mass spectrometer, as described.[7a]

Chromatographic purification of compounds: Compounds **6**–**9** were purified by preparative HPLC on an Agilent 1260 series preparative instrument equipped with a Zorbax Eclipse XDB C_8 column (250×21.2 mm, 10 μm). Solvent A was 0.1% trifluoroacetic acid (TFA) in water, solvent B was ACN. A linear gradient of 5→100% B over 20 min at a flow of 20 mL min^{-1} was applied. Further workup of **6**–**8** included chromatography on an Agilent 1260 series analytical/semipreparative instrument equipped with a ThermoFischer Hypercarb column (150×10 mm, 5 μm, flow: 3 mL min^{-1}). Solvent A was 0.1% (*v/v*) TFA in H_2O, solvent B was ACN. The gradient included an initial hold at 10% B for 1 min, linear increase to 30% B over 1 min, to 60% B over 9 min, and to 100% B over 0.5 min. Final purification was accomplished on a Phenomenex Synergi Polar-RP column (150×4.6 mm, 4 μm, flow: 1.5 mL min^{-1}). The gradient was linear increase 1→10% B over 9 min, and to 100% B over 0.5 min.

NMR spectroscopy: 1D and 2D NMR spectra of **8** were recorded at 300 K on a Bruker Avance III spectrometer at 600 MHz in [D_6]DMSO. Chemical shifts were referenced to residual non-deuterated solvent ($\delta_H = 2.50$ ppm and $\delta_C = 39.5$ ppm).

In silico modeling of PsiM: Homology modeling of PsiM and fully flexible ligand docking of SAM was undertaken in ICM-Pro desktop modeling package v3.8-7b (MolSoft LLC), based on the Internal Coordinates (IC) representation of molecular objects.[20] After initial placement of the aligned polypeptide chain onto the template structure, side-chain torsion angles were predicted by simultaneous global optimization of the energy for all non-identical residues. The conformational modeling of the protein side chains and loops was then refined by using the Biased Probability Monte Carlo (BPMC) optimization method.[21] The SAM binding pocket was prepared for ligand docking,[22] and the ligand was docked by using ICM-Pro.

Acknowledgements

We thank Andrew Perner and Heike Heinecke (Hans-Knöll-Institute Jena), and Florian Baldeweg (Friedrich-Schiller-University, Jena) for recording high-resolution mass and NMR spectra, and for additional interpretation of NMR data, respectively. We are grateful to Professor Dr. Florian P. Seebeck (University of Basel) for expression plasmids to produce S*-adenosylhomocysteine nucleosidase and adenine deaminase. This work was supported by the Deutsche Forschungsgemeinschaft (DFG grant HO2515/7-1 to D.H.) and by the Usona Institute (Madison, WI). D.H. is also supported by the DFG Collaborative Research Center ChemBioSys 1127. B.R. and A.N. receive partial funding from the Austrian Science Fund (FWF) under project P 28395-B26.*

Conflict of Interest

The authors declare no conflict of interest.

Keywords: baeocystin · biosynthesis · enzymes · methyltransferase · psilocybin

[1] a) A. Hofmann, A. Frey, H. Ott, T. Petrzilka, F. Troxler, *Experientia* **1958**, *14*, 397–399; b) A. Hofmann, R. Heim, A. Brack, H. Kobel, A. Frey, H. Ott, T. Petrzilka, F. Troxler, *Helv. Chim. Acta* **1959**, *42*, 1557–1572; c) A. Y. Leung, A. G. Paul, *J. Pharm. Sci.* **1968**, *57*, 1667–1671.

[2] a) D. E. Nichols, *Pharmacol. Ther.* **2004**, *101*, 131–181; b) F. Hasler, U. Grimberg, M. A. Benz, T. Huber, F. X. Vollenweider, *Psychopharmacology* **2004**, *172*, 145–156.

[3] a) C. S. Grob, A. L. Danforth, G. S. Chopra, M. Hagerty, C. R. McKay, A. L. Halberstadt, G. R. Greer, *Arch. Gen. Psychiatry* **2011**, *68*, 71–78; b) M. W. Johnson, A. Garcia-Romeu, M. P. Cosimano, R. R. Griffiths, *J. Psychopharmacol.* **2014**, *28*, 983–992; c) A. Mahapatra, R. Gupta, *Ther. Adv. Psychopharmacol.* **2017**, *7*, 54–56; d) A. M. Sherwood, T. E. Prisinzano, *Exp. Rev. Clin. Pharmacol.* **2018**, *11*, 1–3.

[4] a) F. Troxler, F. Seemann, A. Hofmann, *Helv. Chim. Acta* **1959**, *42*, 2073–2103; b) A. Cerletti, M. Taeschler, H. Weidmann, *Adv. Pharmacol.* **1968**, *6*, 233–246.

[5] a) F. Yamada, M. Tamura, A. Hasegawa, M. Somei, *Chem. Pharm. Bull.* **2002**, *50*, 92–99; b) D. B. Repke, W. J. Ferguson, D. K. Bates, *J. Heterocycl. Chem.* **1981**, *18*, 175–179; c) R. A. Glennon, E. Schubert, J. M. Jacyno, *J. Med. Chem.* **1980**, *23*, 1222–1226.

[6] A. T. Shulgin, A. Shulgin, *Tihkal: The Continuation*, Transform Press, Berkeley, **1997**.

[7] a) J. Fricke, F. Blei, D. Hoffmeister, *Angew. Chem. Int. Ed.* **2017**, *56*, 12352–12355; *Angew. Chem.* **2017**, *129*, 12524–12527; b) J. Fricke, F. Blei, D. Hoffmeister, *Angew. Chem.* **2017**, *129*, 12524–12527; c) H. T. Reynolds, V. Vijayakumar, E. Gluck-Thaler, H. B. Korotkin, P. B. Matheny, J. C. Slot, *Evol. Lett.* **2018**, *2*, 88–101; d) J. Fricke, C. Lenz, J. Wick, F. Blei, D. Hoffmeister, *Chem. Eur. J.* **2019**, *25*, 897–903.

[8] F. Blei, F. Baldeweg, J. Fricke, D. Hoffmeister, *Chem. Eur. J.* **2018**, *24*, 10028–10031.

[9] H. Zalkin, C. Yanofsky, *J. Biol. Chem.* **1982**, *257*, 1491–1500.

[10] R. J. Goss, P. L. Newill, *Chem. Commun.* **2006**, *47*, 4924–4925.

[11] a) A. Vit, L. Misson, W. Blankenfeldt, F. P. Seebeck, *ChemBioChem* **2015**, *16*, 119–125; b) L. Misson, R. Burn, A. Vit, J. Hildesheim, M. A. Beliaeva, W. Blankenfeldt, F. P. Seebeck, *ACS Chem. Biol.* **2018**, *13*, 1333–1342.

[12] F. Blei, J. Fricke, J. Wick, J. C. Slot, D. Hoffmeister, *ChemBioChem* **2018**, *19*, 2160–2166.

[13] B. P. S. Chouhan, S. Maimaiti, M. Gade, P. Laurino, *Biochemistry* **2019**, *58*, 166–170.

[14] H. L. Schubert, R. M. Blumenthal, X. Cheng, *Trends Biochem. Sci.* **2003**, *28*, 329–335.

[15] A. Waterhouse, M. Bertoni, S. Bienert, G. Studer, G. Tauriello, R. Gumienny, F. T. Heer, T. A. P. de Beer, C. Rempfer, L. Bordoli, R. Lepore, T. Schwede, *Nucleic Acids Res.* **2018**, *46*, W296–W303.

[16] J. R. Min, H. Wu, H. Zeng, P. Loppnau, J. Weigelt, M. Sundstrom, C. H. Arrowsmith, A. M. Edwards, A. Bochkarev, A. N. Plotnikov, Structural Genomics Consortium, PDB ID: 2H00, **2006**.

[17] J. E. Audia, D. A. Evrard, G. R. Murdoch, J. J. Droste, J. S. Nissen, K. W. Schenck, P. Fludzinski, V. L. Lucaites, D. L. Nelson, M. L. Cohen, *J. Med. Chem.* **1996**, *39*, 2773–2780.

[18] H. Harada, Y. Hirokawa, K. Suzuki, Y. Hiyama, M. Oue, H. Kawashima, N. Yoshida, Y. Furutani, S. Kato, *Bioorg. Med. Chem. Lett.* **2003**, *13*, 1301–1305.

[19] a) O. Shirota, W. Hakamata, Y. Goda, *J. Nat. Prod.* **2003**, *66*, 885–887; b) D. E. Nichols, S. Frescas, *Synthesis* **1999**, *6*, 935–938; c) J. Gartz, *J. Basic Microbiol.* **1989**, *29*, 347–352; d) P. Catalfomo, V. E. Tyler, *Lloydia* **1964**, *27*, 53–63.

[20] R. Abagyan, M. Totrov, D. Kuznetsov, *J. Comput. Chem.* **1994**, *15*, 488–506.

[21] R. Abagyan, M. Totrov, *J. Mol. Biol.* **1994**, *235*, 983–1002.

[22] A. J. W. Orry, R. Abagyan in *Homology Modeling: Methods and Protocols* (Eds.: A. J. W. Orry, R. Abagyan), Humana, Totowa, **2012**, pp. 351–373.

Manuscript received: May 31, 2019
Accepted manuscript online: May 31, 2019
Version of record online: October 17, 2019